

Inertial Separation of Particles Escaped from Electrostatic Precipitators

Liqiang Qi,* Mengmeng Liu, Xu Wang, Jingxin Li, and Fang Zeng

Cite This: *ACS Omega* 2021, 6, 10875–10883

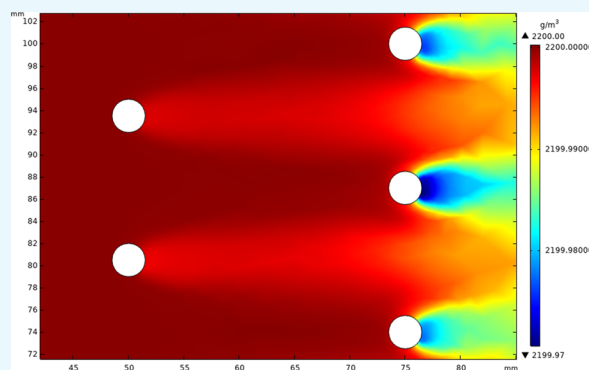
Read Online

ACCESS |

Metrics & More

Article Recommendations

ABSTRACT: For particles that escape from electrostatic precipitators (ESPs), inertial recapture is used to improve the efficiency of dust removal. A rod-grid inertial separator was designed. The electrostatic and fluid flow particle tracking modules were selected in the model established by the COMSOL software, and the dust removal efficiency of the proposed dust separator was evaluated. When the flue gas velocity was $20 \text{ m}\cdot\text{s}^{-1}$, the diameter of the round rod was 8 mm, and the spacing of the pipes was 15 mm, the removal efficiency of PM_{2.5} and PM₁₀ reached 27.8 and 84.6%, respectively. Experiments were performed under laboratory conditions and actual working conditions in a coal-fired power plant flue. Results showed that an inertial separator can achieve more than 60% efficiency in recapturing fly ashes that have escaped from ESPs. It can effectively remove fine particles and aerosol pollutants represented by PM_{2.5} and PM₁₀.



1. INTRODUCTION

China's environmental protection standards are becoming increasingly strict. The ultralow emission standard of coal-fired power plants has reduced dust emission concentration to $10 \text{ mg}/\text{Nm}^3$.^{1,3} Electrostatic precipitators (ESPs) have been widely applied as a particle collection system for industrial fumes. The fine particle removal characteristics of ESPs have been extensively evaluated and analyzed.^{2,3} Some strict guidelines and particle emission standards have been implemented for controlling fine particle emissions in recent years, especially in China. However, conventional dust removal devices, such as ESPs, cannot meet the new standards.

ESP technology is currently widely used in power plants in China; many cutting-edge technologies have been developed.⁴ A low-temperature (LLT) ESP system has better particle capture efficiency than traditional ESPs.^{5–7} Lower flue gas temperature can increase the breakdown field strength and gas density and reduce the specific resistance of fly ash and flow velocity. Electrostatic agglomeration is one of the effective solutions to improve the collecting efficiency of fine particles.⁸ Agglomeration can connect two or more particles and convert them into a larger particle, which can be removed from the flue gas by conventional dust removal technology.⁹ Moreover, turbulent agglomeration relies on fluid flow and interparticle collision to prompt the growth and removal of fine particles,^{10–12} and it is a convenient and economical way owing to the simple structures, low cost, reliable operation, and easy retrofitting and maintenance.

Inertial separation of dust escaped from ESPs is a worthwhile means.¹³ In inertial adhesion, dust collection happens when dust hits and adheres to the collecting surface,^{14,15} and a dust layer is formed by adhering the dust particles to one another under the collision of a high flow velocity and then impacting the dust collector.

For particles of a certain size, a critical velocity exists beyond which the particles will bounce back from the surface and not adhere. This velocity depends on the elasticity of the particles and the surface and is inversely proportional to the particle size. When airflow velocity is high, large particles collide with a large elastic force and do not easily adhere. However, a high airflow velocity is advantageous for capturing fine particles. When particles bounce, the sedimentation coefficient increases.¹⁶

Dunbar¹⁷ studied cascade impact samplers and found that the main factor affecting the collection efficiency of such samplers is particle rebound, which can be reduced by applying a thin layer of grease on the impact plate. Demokritou¹⁸ experimented with the use of polyurethane foam impingement plates and found that even if the surface of the plates is not

Received: February 3, 2021

Accepted: March 31, 2021

Published: April 13, 2021



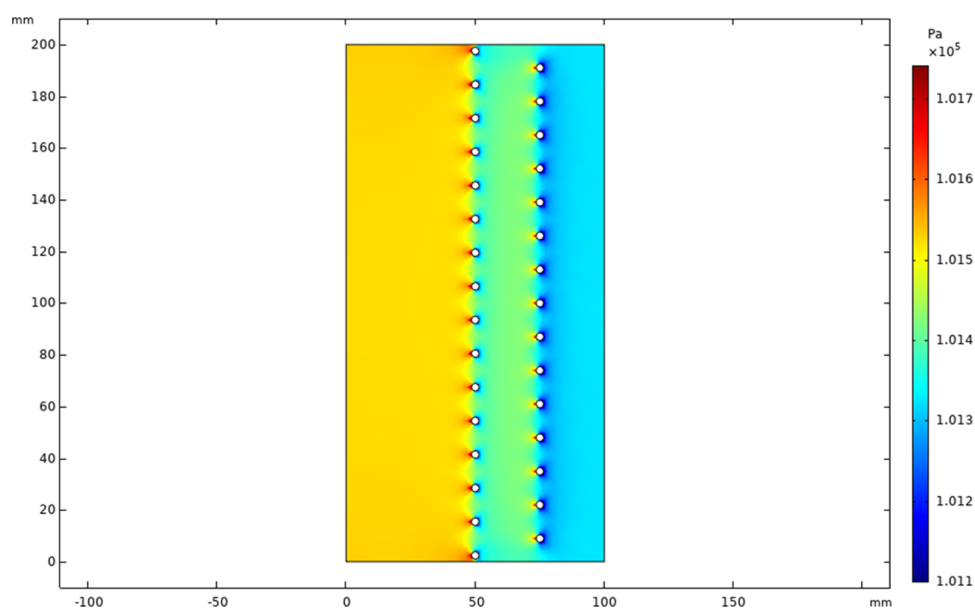


Figure 1. Flow diagram of internal pressure change of the rod-grid inertial separator.

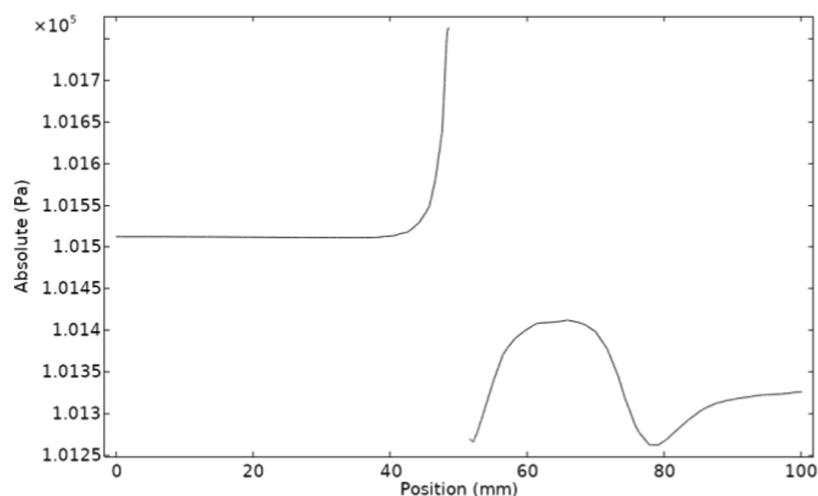


Figure 2. Pressure curve of the rod-grid inertial separator.

coated with grease and other adhesive substances, particles rarely rebound into the air stream.

A related research indicates that inertial adhesion is limited to the application of a sampler and has yet to be studied as a dust removal device. Research results reveal that a sampler cannot be used as a dust collector directly in industrial dust removal. Therefore, a dust removal technology based on inertial adhesion theory must be developed.^{19–21}

Inertial separators are characterized by simple designs, low investment and operating costs, and a high reliability. The inertial particle separator is widely used as an important gas–solid separation device to protect the core engine in a severely polluted environment.^{22–24} The separation efficiency of the IPS is not only affected by the single geometrical or aerodynamic parameter but also apparently influenced by the interaction effects between different parameters. In the inertial separator, the trajectories of particles with small size are dominated by the flow direction while the paths of particles with larger size are dominated by the individual particle inertia and bounce characteristics from the walls. In general, a high flow velocity is conducive to the inertial separation of particles,

while a slower flow velocity increases the collection efficiency of ESPs. The inertial separator and ESPs are connected in series, and high collection efficiency will be acquired at low and high velocities. Thus, the topic of inertial separation of particles from ESPs is new and can fill the knowledge gap on this subject. This work focuses on particles that have escaped from the tail of ESPs of thermal power plants. The objective is to find a new solution to meet the national emission standards by capturing particles through an inertial adhesion mechanism under a high flow rate condition and to further reduce the dust emission concentration. Due to low pressure drop and high efficiency, air cleaners based on ESPs have also been widely applied to remove fine particles and improve indoor and outdoor air quality.^{25–27} Thus, this study can be used to guide the removal of indoor and outdoor particles by joint electrostatic inertial separators.

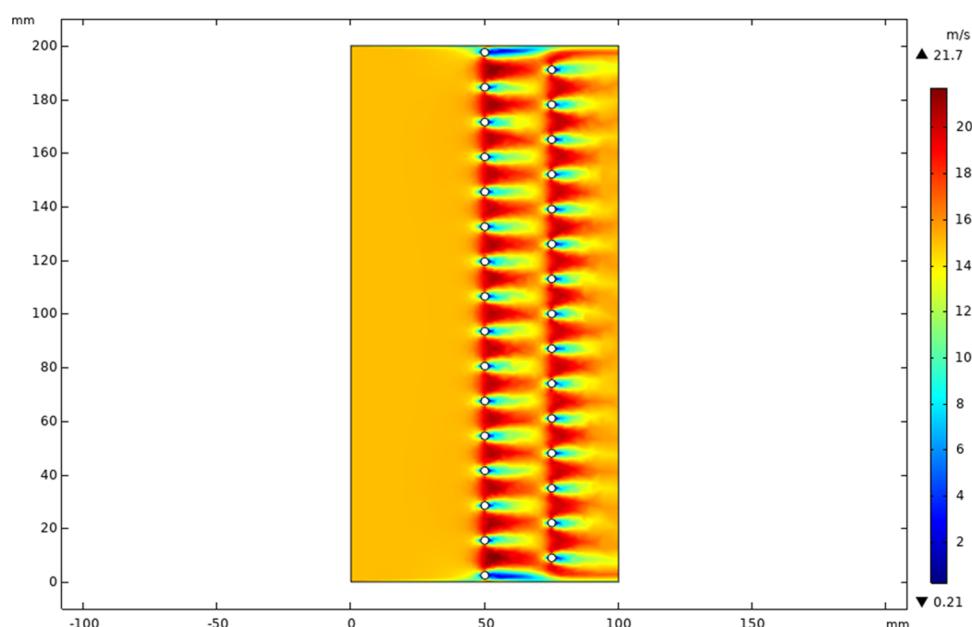


Figure 3. Simulated velocity field of the rod-grid inertial separator.

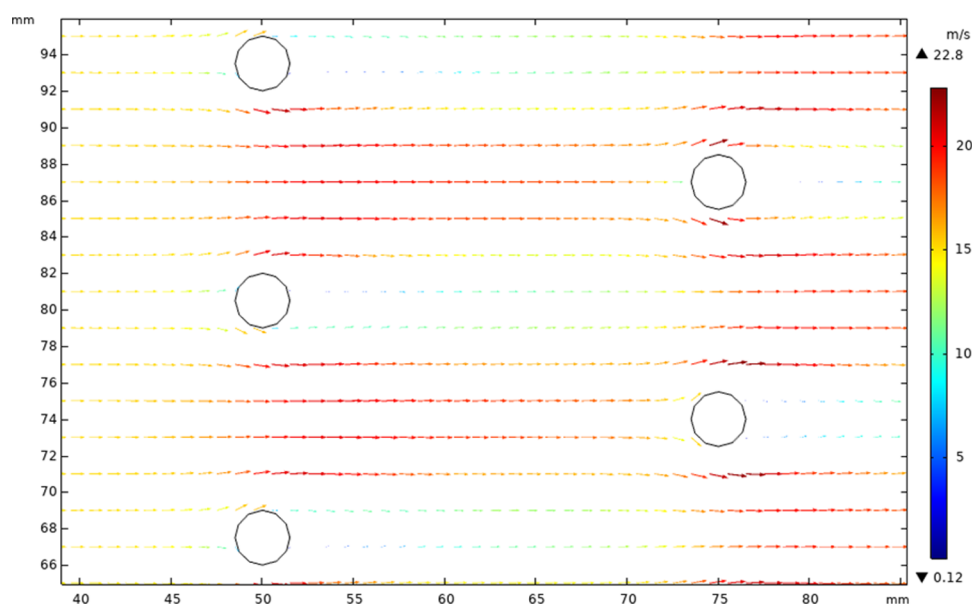


Figure 4. Flow field variation inside the rod-grid inertial separator.

2. RESULTS AND DISCUSSION

2.1. Computational Modeling Results. **2.1.1. Simulated Pressure Field.** Figure 1 shows the pressure loss of the rod-grid inertial separator. The velocity is $15 \text{ m}\cdot\text{s}^{-1}$.

The cloud diagram in Figure 1 and the graph in Figure 2 show that the pressure drop from the inlet to outlet is about 200 Pa, much lower than that of the particle filter. Moreover, after the airflow passes through a row of impact rods, the pressure is greatly reduced, and the pressure between the two rows of plates is relatively stable. This result is attributed to the sudden contraction and expansion that occur when the airflow passes the impact rods, thus causing a sudden change in the velocity of the airflow. This change in airflow velocity causes a change in pressure, which is the impact after each row.

2.1.2. Simulated Velocity Field. The simulated velocity field of the rod-grid inertial separator is shown in Figure 3.

Figure 3 illustrates that when the circular rod is hit, the area of the fluid flow suddenly shrinks and expands, increasing the flow velocity at the gap between the round rods in each row of rods. On the side of the round pipe facing the airflow, the gas velocity is low, that is, only $\sim 9 \text{ m}\cdot\text{s}^{-1}$. Meanwhile, the flow rate on the back side of the rod is low, and eddy currents are generated. In a turbulent flow field, fine particles collide and agglomerate with each other under the influence of vortices, which can improve the removal efficiency of fine particles.

2.1.3. Changes in the Flow Field. The flow field variation inside the rod-grid inertial separator is shown in Figure 4.

Airflow impinges on the collecting round bar at a certain velocity. The velocity of the airflow is higher around the round rod, which is favorable for the inertial adhesion of dust. Then, the airflow flows around the collecting round bar, exhibiting an acceleration process. A low-speed vortex area is formed on the

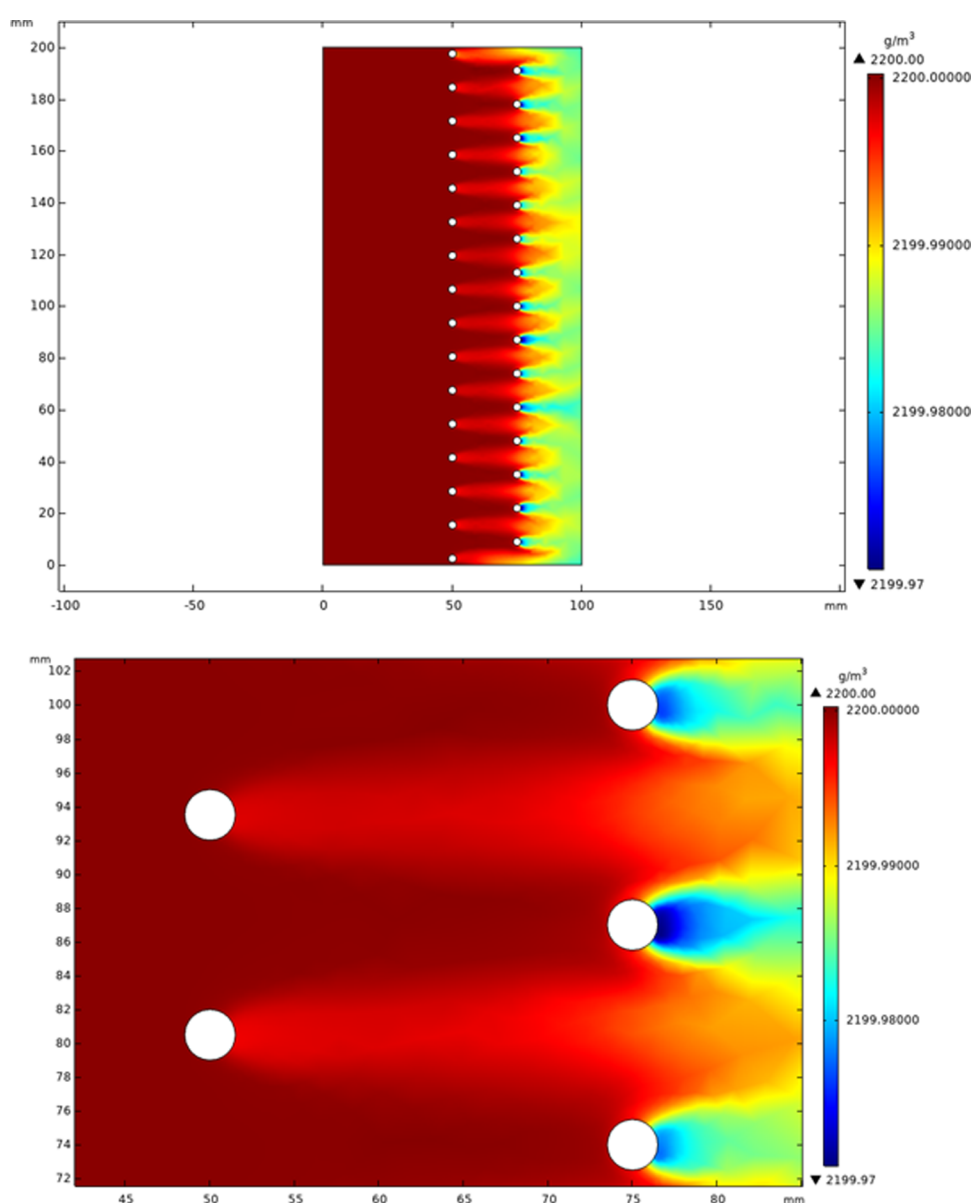


Figure 5. Concentration distribution of dust in the rod-grid inertial separator.

back convection surface of the round bar, and some dust can also be collected, which improves the dust removal efficiency.

2.1.4. Simulated Dust Concentration Cloud Map. The concentration distribution of dust in the rod-grid inertial separator was simulated. The dust concentration at the inlet of the device is 2200 mg/m^3 , the particle size is $10 \text{ }\mu\text{m}$, and the velocity is $15 \text{ m}\cdot\text{s}^{-1}$.

Figure 5 shows that the concentration of dust in the entire flow field is relatively uniform. On the upstream surface of the trapping rod, dust concentration reaches the maximum owing to the adhesion and trapping of dust.

2.1.5. Simulated Particle Trajectory Map. The rod-grid inertial separator has a gas–solid two-phase flow field. In addition to the distribution of the gas flow field, the trajectory of the particle phase is also a research focus. Figure 6 illustrates the particle trajectories in the rod-grid inertial separator under different velocities. Figure 7 shows the trajectories of 2.5 and $10 \text{ }\mu\text{m}$ particles in the rod-grid inertial separator at 18 m/s velocity. The figure indicates that the trajectory of the particle phase in the flow field away from the trapping rod is relatively

regular, that is, the flow field can be regarded as being in a laminar flow state. Impact, flow, acceleration, and deceleration occur in the vicinity of the trapping rod, and some eddy currents appear. Small-scale vortices were more conducive to the removal of fine particles.

In the case of different velocities, the particle trajectory does not change significantly and only affects the internal turbulence.

2.2. Simulated Dust Removal Efficiency. Evaluating the removal efficiency of particles in flue gas is important for engineering practice.

Figure 8 presents the simulation results for the collection efficiencies of particles with diameters of 0.1, 0.5, 1, 2.5, 5, and $10 \text{ }\mu\text{m}$ at flow velocities of $10\text{--}20 \text{ m}\cdot\text{s}^{-1}$. The collection efficiency increased with the increase of flow velocity and particle size. The particle trajectories with small particle size, because of the relatively smaller inertia, are dominated by the flow direction, while paths with larger particle size are dominated by the individual particle inertia and bounce characteristics from the rods. The inertial forces acting on

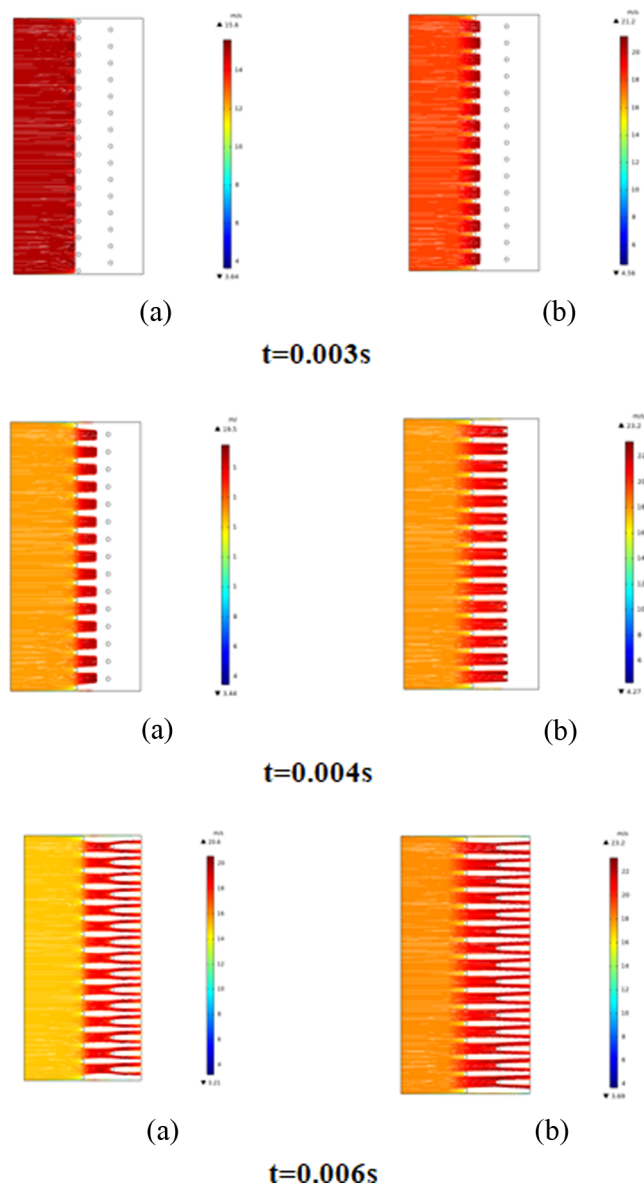


Figure 6. Particle trajectories in the rod-grid inertial separator under different velocities: (a) 15 m/s and (b) 18 m/s.

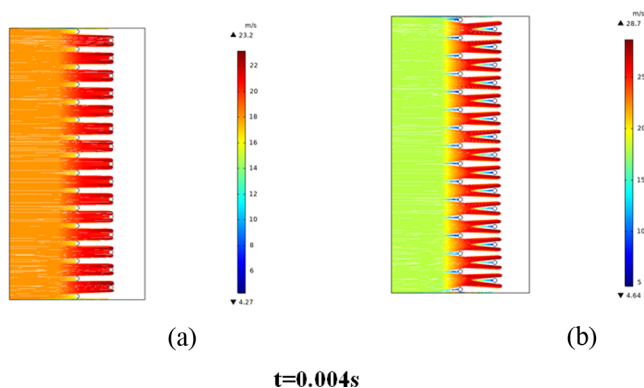


Figure 7. Trajectories of (a) 2.5 and (b) 10 μm particles at 18 m/s.

particles are larger with higher velocities. When the particles flow around the rod, large inertial forces make it more difficult for the particles to change their direction of motion.

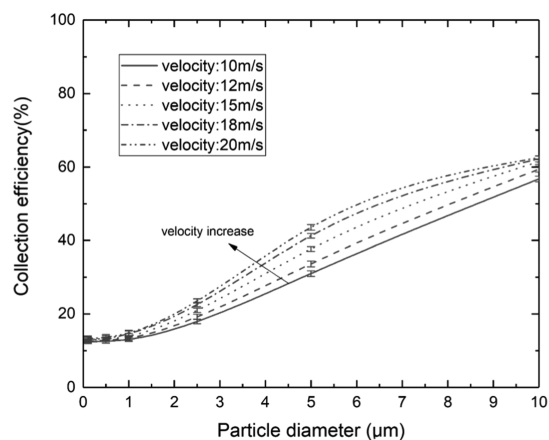


Figure 8. Simulated collection efficiencies of the inertial separator according to flow velocity.

Figures 9 and 10 show the collection efficiencies of particles with round rod diameters of 3, 5, and 8 mm, and rod distances

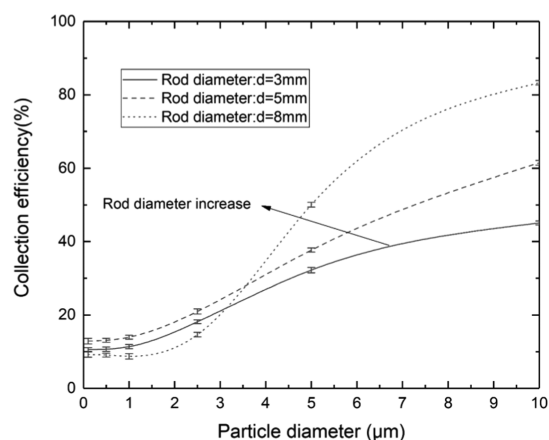


Figure 9. Simulated collection efficiencies of the inertial separator with different rod diameters.

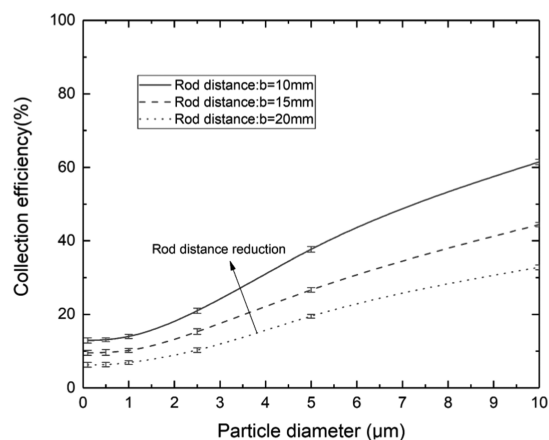


Figure 10. Simulated collection efficiencies of the inertial separator with different rod distances.

of 10, 15, and 20 mm. When the particle size was larger than 2.5 μm , the collection efficiency of the inertial separator increased as the rod diameter increased (Figure 9). Because large particles have larger inertial forces and the blocking area increases with the increase of rod diameter, the probability of

particle capture increases accordingly. Small particles have a relatively smaller inertia, and it is easier to get around the rod with the flow. For all particle sizes, the collection efficiency decreased with the increase of rod distance (Figure 10). Combination of the electrostatic precipitator and inertial separator is more effective for collecting large particles than turbulent agglomeration. The collection efficiency of PM_{2.5} and PM₁₀ can reach 27.8 and 84.6%, respectively. For PM_{2.5}, the capture efficiency of 27.8% combined with the fractional PM removal efficiency of the WFGD after ESP will meet the ultralow emission standard.

A slower flow velocity can increase the collection efficiency of ESPs, while a faster flow velocity can increase the collection efficiency of inertial dust separators. When these types of dust collectors are connected in series, a high collection efficiency can be expected at both low and high velocities. Moreover, both the precharge of the ESP and the turbulence of the inertial separator can improve the collection efficiency of particles.

2.3. Laboratory Experiments. According to the simulation results, rods with a diameter of 8 mm and a distance of 10 mm were selected in the laboratory experiment.

Table 1 indicates that, for 10 g of ash fed at different gas velocities for 60 min, the amount of ash collected by the trap

Table 1. Efficiency of Dust Collection at Different Gas Velocities

wind speed (m/s)	10	12	15	18
dust collection (g)	1.604	2.356	2.842	3.648
collection efficiency (%)	16.04	23.56	28.42	36.48
standard deviation (%)	1.10	1.42	0.99	1.26

increases with increasing velocity. The total removal efficiency of the experimental and simulation results matches well under all flow velocity conditions, but its value found in the experiment is lower than the simulation predictions. One reason is that a large amount of ash samples is present at the bottom of the pipeline because this area is small, the distance from the feed port to the trap gate is short, and the airflow velocity is low. Thus, the ash sample cannot be completely suspended after it comes down from the feed port and a large part falls at the bottom of the pipe. Moreover, because the feed port is too close to the trap, the ash sample coming down from the feed port is not evenly dispersed in the gas stream.

With the 18 m·s⁻¹ gas velocity, the change of ash collection on the round rod with time (10, 20, 30, and 60 min) is observed. The ash samples from the surfaces are weighed. The results are shown in Table 2.

Table 2. Amount of Dust Collected over Time

time (min)	10	20	30	60
rod ($\Phi = 5$ mm)	0.793	1.886	2.662	2.726
rod ($\Phi = 8$ mm)	1.321	2.609	3.586	3.648
standard deviation (%)	1.15	1.20	1.01	1.05

According to the amount of dust collected, as dust collection time increases, the dust collected from the round pipe also increases but the flow area of the round pipe remains constant. Moreover, the amount of dust carried by the round pipe has a maximum value, which is impossible to increase without limit.

When the stainless steel rod is placed in the flue for 10 min, a thin layer of dust adheres to the surface of the rod, which is evenly distributed along the surface of the pipe facing the airflow. The dust that adheres on the rod for 20 min increases compared to that on the rod for 10 min, and the dust collected in the middle portion of the round rod facing the airflow surface increases. After adherence for 30 min, the dust on the round rod increases further and the accumulated dust forms a cone shape. After standing for 60 min, the dust collected by the round rod continues to increase further but only slightly. Therefore, after 30 min of dust collection, the dust collected on the round pipe is near the maximum load of the round pipe. Increasing the dust collection time does not improve dust collection greatly.

2.4. Field Experiments. Field tests are conducted in a thermal power plant in North China.

The dust concentration of flue gas from the outlet of ESP is 56.8 mg/Nm³, flue gas moisture content is 4.5%, flue gas flow velocity is 20.4 m·s⁻¹, flue gas temperature is ~145 °C, and SO₂ concentration is 1.02%. The pipeline negative pressure is -2670 Pa.

The rod-grid inertial separator was placed in the flue behind the outlet of ESP. The image of the rod after particle collection for 30 min is shown in Figure 11.

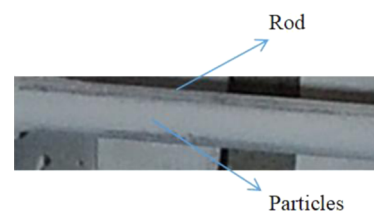


Figure 11. Image of the rod after dust collection for 30 min.

After 30 min, the dust concentration at the outlet of flue was 21.3 mg/m³. Thus, the collection efficiency of the rod-grid inertial separator can reach 62.5%. It is an effective way to reduce particulate emissions and does not require a major overhaul.

3. CONCLUSIONS

A rod-grid inertial separator after ESPs was designed. An analysis of pressure change in the rod-grid inertial separator indicates that the change in flow velocity, trajectory of the dust particles, and some rules about the operation of the rod-grid inertial separator have been obtained. The dust removal efficiency of the proposed dust separator was evaluated. When the flue gas velocity was 20 m·s⁻¹, the diameter of the round rod was 8 mm, and the spacing of the pipes was 15 mm, the removal efficiency of PM_{2.5} and PM₁₀ reached 27.8 and 84.6%, respectively. Experiments were performed under laboratory conditions and field working conditions in a coal-fired power plant flue. The law of experimental and simulation results matched well under all flow velocity conditions. Field experiments showed that the inertial separator can achieve 62.5% efficiency in recapturing fly ashes that have escaped from ESPs. Inertial separation of particles escaped from ESPs is a new solution to meet national emission standards and to reduce the dust emission concentration.

4. MATERIALS AND METHODS

4.1. Experimental Setup and Instrumentation.

4.1.1. Experimental System. A schematic diagram of the flue retrofit used in the laboratory is shown in Figure 12. The

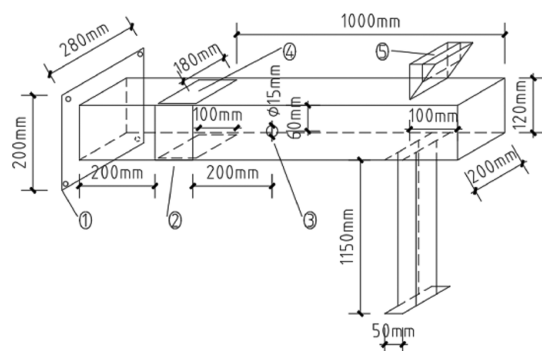


Figure 12. Diagram of the flue retrofit used in the laboratory: ①, flange; ②, trapping grate segment; ③, side wall openings; ④, open pore; and ⑤, hopper.

diameter of the flue in the laboratory is 400 mm, and the flow rate of the regulated airflow can only reach $\sim 8 \text{ m}\cdot\text{s}^{-1}$, which is extremely low. Therefore, another small tube is designed, fabricated, and installed. This tube is connected to the small rectangular observation hole on the side of the dust removal tube and blocks the inlet of this tube. Owing to the reduced airflow area, the gas flow rate in the small tube can be increased up to $18 \text{ m}\cdot\text{s}^{-1}$.

After the test rig is connected to the dust removal tube, the collecting rod is arranged in the trapping grid section. There are two rows of collecting rods interlaced in the direction of vertical airflow (Figure 13, top view).

4.1.2. Laboratory Experiments. The dust removal efficiency of the precipitator is tested in the laboratory.

The angle of the wind deflector is adjusted to change the gas velocity, which is measured with a hot-ball anemometer.

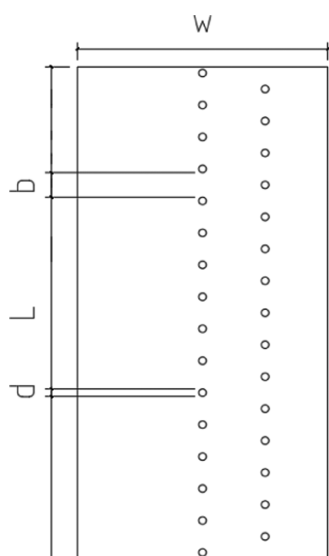


Figure 13. Arrangement of the collecting rods in the trapping grid section: w , the width of the trapping grid section; L , the length of the trapping grid section; b , distance between collecting rods; and d , rod diameter.

Experimental gas velocities of 10, 12, 15, and $18 \text{ m}\cdot\text{s}^{-1}$ for 10 g of ash fed into the flue in front of the inertial separator by the automatic feeder are recorded. The experiment lasts for 30 min, and the amount of ash collected on the surface of the rod is weighed.

Fly ashes have been obtained from the dust hopper of ESP in the Tuoketuo Power Plant, China. A YFJ Bahco centrifuge (Chengde Instrument and Meter Factory) was used to measure the size distributions of fly ashes. The dispersity of fly ash is shown in Figure 14.

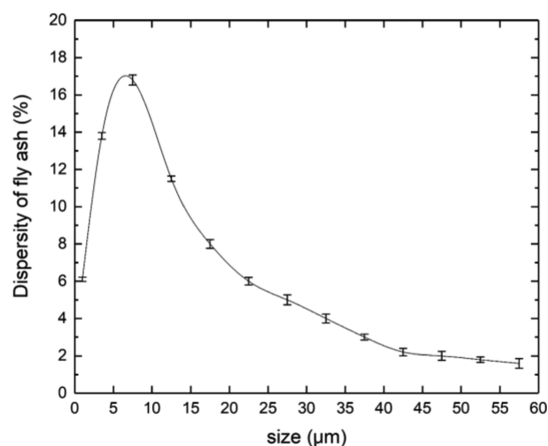


Figure 14. Dispersity of the fly ash.

The collection efficiencies have been calculated as follows

$$\eta = \left(1 - \frac{M_{\text{passed}}}{M_{\text{total}}} \right) \times 100\% = \frac{M_{\text{trapped}}}{M_{\text{total}}} \times 100\% \quad (1)$$

where M_{passed} is the mass concentration of particles leaving the inertial separator through the outlet, M_{trapped} is the mass concentration of particles trapped by rods, and M_{total} is the mass concentration of particles fed at the inlet. An isokinetic sampling method was used for the measurement of the mass concentration of particles.

4.1.3. Test under Real Conditions. Field tests were performed in a power plant.

Boilers (410 tons) of 50 MW capacity were running in the thermal power plant in North China. The dust concentration of flue gas is $216 \text{ mg}/\text{Nm}^3$, dust collector efficiency is 99.54%, flue gas moisture content is 4.5%, flue gas flow rate is $15.4 \text{ m}\cdot\text{s}^{-1}$, flue gas temperature is $\sim 145 \text{ }^\circ\text{C}$, and SO_2 concentration is 1.02%. The pipeline negative pressure is -2670 Pa .

In the field experiment of power plant A#5, sample devices are inserted into the holes at the side of the downstream flue and left for 10, 20, 30, and 60 min. The ash on the round rod is observed. In the field test, owing to the high flow rate in the flue gas pipeline and the lower pressure in the flue in comparison with the atmospheric pressure, measures must be taken to prevent air from leaking out from the measuring hole. Such measures, which include washing the stainless steel pipe, affect the dust collection efficiency.

The dust collected from the stainless steel rods is brought back to the laboratory for weighing.

Total mass concentrations of particles at the entrance and exit of the ESP were simultaneously measured, and an isochronic sampling method was used for the particulate

matter sample (Methods of Performance Tests for Electrostatic Precipitators, GB/T13931-2002 of China).

4.2. Simulation Approach and Numeric Computation.

4.2.1. Theoretical Model. Given that the diameter of the particles used for calculations is larger than the average free path of gas molecules, the particles must not be treated as “quasifluid”. In the present study, the influence of the electric field on the flow field is usually neglected in the numerical simulation. The airflow through the ESP channel is modeled as steady and turbulent while assuming constant density and viscosity.²⁸ Therefore, the discrete phase model (DPM) (i.e., Euler–Lagrange model) is adopted to simulate particle flow in the transverse-plate ESP.

In calculating the single-phase flow field, the gas is assumed to be complete, with a constant specific heat coefficient that ignores mass force and viscosity.

- (1) Gas-phase control equation: For the 3-D compressible two-phase flow field of the transverse-plate ESP, the general form of the conservation equations of the gas phase in the Euler coordinate system is

$$\begin{aligned} \frac{\partial}{\partial x}(\rho u \phi) + \frac{1}{r} \frac{\partial}{\partial r}(r \rho v \phi) \\ = \frac{\partial}{\partial x} \left(\Gamma_{\phi} \frac{\partial \phi}{\partial x} \right) + \frac{1}{r} \frac{\partial}{\partial r} \left(r \Gamma_{\phi} \frac{\partial \phi}{\partial r} \right) + S_{\phi} + S_{p\phi} \end{aligned} \quad (2)$$

where u is the gas velocity, v is the velocity of the particle, ϕ is any independent variable, Γ_{ϕ} is the transport coefficient, S_{ϕ} is the gas source term, and $S_{p\phi}$ is the source term for the interaction of gas and particles.

- (2) Particle-phase control equation: The equation of the particle phase in the Lagrangian coordinate system is

$$N_k = \int_A n_k v_{kn} dA = \text{const} \quad (3)$$

where A is the cross-sectional area of the channel and v_{kn} is the particle flow rate perpendicular to the component of the flow rod cross section.

When only the fluid resistance and gravity of the particles are considered and other forces and mass loss rates are ignored, the momentum equation of the particle phase in the i direction is

$$\frac{dv_{ki}}{dt} = (v_i - v_{ki})/\tau_{rk} + g_i \quad (4)$$

where τ_{rk} is the particle relaxation time and g_i is the gravitational acceleration.

4.2.2. Flow Field Performance. The COMSOL5.4 software was used in this study to measure and calculate the electrostatic and flow field models of 3-D gas–solid two-phase flow of a rod-grid inertial separator. The collecting rods are round with diameters of 3, 5, and 8 mm, and the distances between the rods are set as 10, 15, and 20 mm, respectively. The gas velocity is controlled at 10, 12, 15, 18, and 20 m·s⁻¹, and the gas velocity data curve is plotted.

In this study, the discrete phase model (DPM) is used to simulate the two-phase flow field of a rod-grid inertial separator. The mesh division is shown in Figure 15.

Initial conditions and boundary conditions: operating pressure: 101 325 Pa; entrance conditions: $V = 15 \text{ m}\cdot\text{s}^{-1}$ (the tail flue gas velocity after the outlet of the ESP); and wall condition: fixed heat flow is 0, no slip wall surface is used, pressure is extrapolated from the value in the flow field, and the

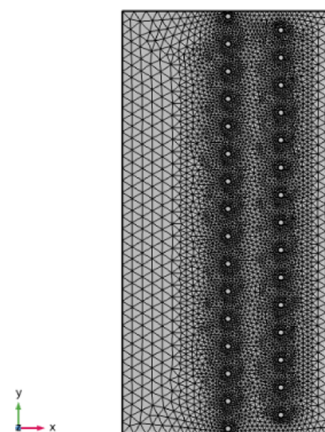


Figure 15. Mesh division of the rod-grid inertial separator.

velocity of particles near the wall is 0, that is, the dust reaches the plate and is completely collected.

4.2.3. Evaluation of Dust Removal Efficiency. The rod-grid inertial separator is designed to remove the particles in the flue gas at the end of ESPs of the coal-fired power plant to realize deep purification of the flue gas.

The electrostatic and fluid flow particle tracking modules are selected in the model established by the COMSOL software. The particles flow with the flow field, and the particle diameter, density, stress (gravity, drag, and electric field), and charging characteristics are set (hypothesis for the saturation charge). The internal wall surface characteristics of the dust collector are also set.

The number and frequency of particle placement are also set. One thousand particles are delivered once every 0.01 s with a delivery time of 1 s. The gas velocity at the inlet of the precipitator is set, and the internal flow field of the precipitator is calculated. Finally, the dust removal efficiency of the precipitator can be obtained according to the number of frozen particles on the flue gas outlet surface of the precipitator combined with the number of particles placed in the flue gas inlet.

■ AUTHOR INFORMATION

Corresponding Author

Liqiang Qi – Hebei Key Laboratory of Power Plant Flue Gas Multi-Pollutants Control, Department of Environmental Science and Engineering, North China Electric Power University—Baoding Campus, Baoding 071003, P. R. China; orcid.org/0000-0001-6039-1224; Phone: +86 13933270460; Email: qiliqiang@ncepu.edu.cn

Authors

Mengmeng Liu – Hebei Key Laboratory of Power Plant Flue Gas Multi-Pollutants Control, Department of Environmental Science and Engineering, North China Electric Power University—Baoding Campus, Baoding 071003, P. R. China

Xu Wang – Hebei Key Laboratory of Power Plant Flue Gas Multi-Pollutants Control, Department of Environmental Science and Engineering, North China Electric Power University—Baoding Campus, Baoding 071003, P. R. China

Jingxin Li – Hebei Key Laboratory of Power Plant Flue Gas Multi-Pollutants Control, Department of Environmental Science and Engineering, North China Electric Power University—Baoding Campus, Baoding 071003, P. R. China

Fang Zeng – Hebei Key Laboratory of Power Plant Flue Gas Multi-Pollutants Control, Department of Environmental Science and Engineering, North China Electric Power University—Baoding Campus, Baoding 071003, P. R. China

Complete contact information is available at:

<https://pubs.acs.org/10.1021/acsoomega.1c00624>

Notes

The authors declare no competing financial interest.

ACKNOWLEDGMENTS

This work was supported by the Natural Science Foundation of Hebei Province (Grant Number B2019S02067) and the Fundamental Research Funds for the Central Universities (Grant Number 2020MS152).

REFERENCES

- (1) Sui, Z.; Zhang, Y.; Peng, Y.; Norris, P.; Cao, Y.; Pan, W. P. Fine particulate matter emission and size distribution characteristics in an ultra-low emission power plant. *Fuel* **2016**, *185*, 863–871.
- (2) Liu, X. W.; Xu, Y. S.; Zeng, X. P.; Zhang, Y.; Xu, M. H.; Pan, S. W.; Zhang, K.; Li, L.; Gao, X. P. Field Measurements on the Emission and Removal of PM_{2.5} from Coal-Fired Power Stations: 1. Case Study for a 1000 MW Ultrasupercritical Utility Boiler. *Energy Fuels* **2016**, *30*, 6547–6554.
- (3) Liu, X. W.; Xu, Y. S.; Fan, B.; Lv, C.; Xu, M. H.; Pan, S. W.; Zhang, K.; Li, L.; Gao, X. P. Field Measurements on the Emission and Removal of PM_{2.5} from Coal-Fired Power Stations: 2. Studies on Two 135 MW Circulating Fluidized Bed Boilers Respectively Equipped with an Electrostatic Precipitator and a Hybrid Electrostatic Filter Precipitator. *Energy Fuels* **2016**, *30*, 5922–5929.
- (4) Molchanov, O.; Krpec, K.; Horak, J. Electrostatic precipitation as a method to control the emissions of particulate matter from small-scale combustion units. *J. Cleaner Prod.* **2020**, *246*, No. 119022.
- (5) Jaworek, A.; Krupa, A.; Czech, T. Modern electrostatic devices and methods for exhaust gas cleaning: a brief review. *J. Electrostat.* **2007**, *65*, 133–155.
- (6) Sui, Z. F.; Zhang, Y. S.; Peng, Y.; Norris, P.; Cao, Y.; Pan, W. P. Fine particulate matter emission and size distribution characteristics in an ultra-low emission power plant. *Fuel* **2016**, *185*, 863–871.
- (7) Grass, N.; Hartmann, W.; Klockner, M. Application of different types of high voltage supplies on industrial electrostatic precipitators. *IEEE Trans. Ind. Appl.* **2004**, *40*, 1513–1520.
- (8) Sobczyk, A. T.; Marchewicz, A.; Krupa, A.; Jaworek, A.; Czech, T.; Kluk, D.; Ottawa, A.; Charchalis, A.; et al. Enhancement of collection efficiency for fly ash particles (PM_{2.5}) by unipolar agglomerator in two-stage electrostatic precipitator. *Sep. Purif. Technol.* **2017**, *187*, 91–101.
- (9) Lin, W. Y.; Hsiao, T. C.; Hong, B. L. Improving the removal efficiency of fine particulate matters in air pollution control devices: Design and performance of an electrostatic aerosol particle agglomerator. *J. Taiwan Inst. Chem. Eng.* **2020**, *107*, 110–118.
- (10) Woo, S. H.; Cheon, T. W.; Lee, G.; Kim, J. B.; Bae, G. N.; Kwon, S. B.; Jang, H. R.; Yook, S. J. Performance evaluation of a hybrid dust collector for removing particles during subway train operation. *Aerosol Sci. Technol.* **2019**, *53*, 562–574.
- (11) Chen, D. L.; Wu, K.; Mi, J. C. Experimental investigation of aerodynamic agglomeration of fine ash particles from a 330 MW PC-fired boiler. *Fuel* **2016**, *165*, 86–93.
- (12) Sun, Z. K.; Yang, L. J.; Shen, A.; Zhou, L.; Wu, H. Combined effect of chemical and turbulent agglomeration on improving the removal of fine particles by different coupling mode. *Powder Technol.* **2019**, *344*, 242–250.
- (13) Sun, Z. K.; Yang, L. J.; Wu, H.; Wu, X. Agglomeration and removal characteristics of fine particles from coal combustion under different turbulent flow fields. *J. Environ. Sci.* **2020**, *89*, 113–124.
- (14) Zheng, S.; Zeng, X.; Qi, C.; Zhou, H. Modeling of ash deposition in a pulverized-coal boiler by direct simulation Monte Carlo method. *Fuel* **2016**, *184*, 604–612.
- (15) Larsson, T.; Kjellander, J. A. P.; Överstam, H. “Aerosoltrap”—A New Device for Inertial Dust Separation: CFD Simulations with Experimental Validation. *Part. Sci. Technol.* **2013**, *31*, 221–225.
- (16) Ratynskaia, S.; Vignitchouk, L.; Toliás, P.; Bykov, I.; Bergsaker, H.; Litnovsky, A.; den Harder, N.; Lazzaro, E. Migration of tungsten dust in tokamaks: role of dust-wall collisions. *Nucl. Fusion* **2013**, *53*, No. 123002.
- (17) Dunbar, C.; Kataya, A.; Tiangbe, T. Reducing bounce effects in the Andersen cascade impactor. *Int. J. Pharm.* **2005**, *301*, 25–32.
- (18) Demokritou, P.; Lee, S. J.; Ferguson, S. T.; Koutrakis, P. A compact multistage (cascade) impactor for the characterization of atmospheric aerosols. *J. Aerosol Sci.* **2004**, *35*, 290–299.
- (19) Huang, C. H.; Alonso, M. Influence of particle location on the number of charges per charged nanoparticle at the outlet of a needle charger. *J. Air Waste Manage. Assoc.* **2012**, *62*, 87–91.
- (20) Wang, J.; Wang, X.; Zhu, T.; Zhao, Y. Experimental study on the impact of electrostatic effect on the movement of charged particles. *J. Electrostat.* **2018**, *94*, 14–20.
- (21) Panjwani, B.; Olsen, J. E. Design and modelling of dust capturing system in thermally stratified flowing conditions. *Build. Environ.* **2020**, *171*, No. 106607.
- (22) Zhou, L.; Wang, Z.; Shi, J. Optimization Design of the Integral Inertial Particle Separator Based on Response Surface Method. *J. Appl. Fluid Mech.* **2020**, *13*, 133–145.
- (23) Chen, N. L.; Du, J. M.; Hu, Y. P.; Ji, H. H.; Yuan, Y. Q. Study of the flow and impingement of water droplets inside an inertial particle separator. *AIP Adv.* **2020**, *10*, No. 045313.
- (24) Palumbo, J.; Navi, M.; Tsai, S. S. H.; Speltz, J. K.; Papini, M. Inertial particle separation in helical channels: A calibrated numerical analysis. *AIP Adv.* **2020**, *10*, No. 125101.
- (25) Xiong, W. L.; Lin, Z. P.; Zhang, W. Y.; Chen, T. Z.; Zhao, C. Y. Experimental and simulation studies on dust loading performance of a novel electrostatic precipitator with dielectric barrier electrodes. *Build. Environ.* **2018**, *144*, 119–128.
- (26) Zuraimi, M. S.; Tham, K. W. Reducing particle exposures in a tropical office building using electrostatic precipitators. *Build. Environ.* **2009**, *44*, 2475–2485.
- (27) Kim, H. J.; Han, B.; Kim, Y. J.; Oda, T.; Won, H. Submicrometer particle removal indoors by a novel electrostatic precipitator with high clean air delivery rate, low ozone emissions, and carbon fiber ionizer. *Indoor Air* **2013**, *23*, 369–378.
- (28) Dong, M.; Zhou, F.; Zhang, Y. X.; Shang, Y.; Li, S. F. Numerical study on fine-particle charging and transport behaviour in electrostatic precipitators. *Powder Technol.* **2018**, *330*, 210–218.